Hindawi Publishing Corporation
Mathematical Problems in Engineering
Volume 2011, Article ID 340235, 14 pages
doi:10.1155/2011/340235

Research Article

Vibration Attenuation in Rotating Machines Using Smart Spring Mechanism

Aldemir Ap. Cavalini Jr.,[1] Thiago Vianna Galavotti,[2] Tobias Souza Morais,[1] Edson Hideki Koroishi,[1] and Valder Steffen Jr.[1]

[1] *Laboratory of Mechanics and Structures, (LMEst) School of Mechanical Engineering, University of Uberlândia, Uberlândia, MG, Brazil*
[2] *Group of Smart Materials and Structures, (GMSINT) Mechanical Engineering Department, Engineering Faculty of Ilha Solteira, UNESP, Ilha Solteira, SP, Brazil*

Correspondence should be addressed to Aldemir Ap. Cavalini Jr., aacjunior@mecanica.ufu.br

Received 9 July 2010; Accepted 13 October 2010

Academic Editor: Marcelo Messias

This paper proposes a semiactive vibration control technique dedicated to a rotating machine passing by its critical speed during the transient rotation, by using a Smart Spring Mechanism (SSM). SSM is a patented concept that, using an indirect piezoelectric (PZT) stack actuation, changes the stiffness characteristics of one or more rotating machine bearings to suppress high vibration amplitudes. A Genetic Algorithm (GA) optimization technique is used to determine the best design of the SSM parameters with respect to performance indexes associated with the control efficiency. Additionally, the concept of ecologically correct systems is incorporated to this work including the PZT stack energy consumption in the indexes considered for the optimization process. Simulation carried out on Finite Element Method (FEM) model suggested the feasibility of the SSM for vibration attenuation of rotors for different operating conditions and demonstrated the possibility of incorporating SSM devices to develop high-performance ecologic control systems.

1. Introduction

Commonly, rotating machines cross critical speeds during their transient rotation leading the system to undesirable vibration amplitudes. Under this condition, the occurrence of catastrophic failures caused by crack propagation due to the fatigue process is intensified. Therefore, significant research effort has been devoted to the development and improvement of mechanisms capable to attenuate undesirable vibrations in rotating machines [1–3].

The control approaches for rotating machines are clustered into three main categories, namely passive, active, and semi-active techniques. Passive techniques are normally

performed by devices known as absorbers or isolators. These techniques perform typically over a limited frequency bandwidth and, consequently, are unable to adapt their characteristics to changes in the system. Differently, active approaches promise vibration suppression over a broadband of frequencies in which the suppression is performed by incorporating active actuators, such as PZT stacks, magnetic bearings, and electromagnetic actuators to the machine to act directly against the vibratory loads. Unfortunately, successful implementation of these approaches has been limited by displacement capabilities of the piezoelectric actuators and the expensive costs of magnetic bearings [4]. The semi-active techniques represent an alternative solution to these problems. In semi-active approaches, the vibration is attenuated through an indirect manner by changing the structural parameters of the machine, such as damping and/or stiffness. In our days, the implementation of this technique in rotor dynamics is made possible by techniques such as magnetorheological and electrorheological dampers and SSM.

SSM uses an indirect PZT stack actuation to change the stiffness characteristics of the rotating machine to attenuate high vibration amplitudes. This mechanism can be implemented to attenuate a wide range of vibratory loads such as axial, bending, torsion, or a combination of these ones [4]. For bending control purpose, which is the case studied in the present paper, the SSM must be orthogonally arranged in a plane located at the one or more bearings of the rotating machine.

However, this paper presents a numerical simulation to evaluate the effectiveness of the SSM to attenuate high vibration amplitudes of a rotating machine passing by a critical speed during its transient rotation. The system is composed by horizontal flexible shaft with two rigid discs and three bearings. The SSM parameters are optimized using a GA multiobjective optimization technique, so that the objective function includes the simultaneous minimization of the norm and the maximum absolute value of the outputs measured at all the bearings together with the PZT stack energy consumption, in order to improve the control performance. The inclusion of the energy consumption in the minimization process aims at considering a new worldwide trend in machine design, that is, to obtain control systems that are ecologically correct. This relevant concept has attracted the attention of many researches, being Skladanek et al. [5], Guyomar et al. [6], Matichard and Gaudiller [7], and Maslen et al. [8] the examples of recently published papers involving ecologically correct control systems design, in some of them, for rotating machines, namely ecorotors.

2. Rotor Model

The FEM model of a flexible rotor in transient motion is represented by a matrix differential equation that describes the dynamic behavior of the system

$$[M]\{\ddot{x}\} + [D + \dot{\emptyset}G]\{\dot{x}\} + [K + \dot{\emptyset}K_{st}]\{x\} = \{F_{ext}\}, \tag{2.1}$$

where M is the inertia matrix, D is the damping matrix, G is the gyroscopic matrix, K is the stiffness matrix, K_{st} is a stiffness matrix resulting from the transient motion, x is the generalized displacement vector, F_{ext} is the external forces vector, and $\dot{\emptyset}$ is the angular velocity of the rotor [9].

In this paper, the shaft was modeled by using the Timoshenko's beam element with two nodes and four degrees of freedom per node, two displacements, and two rotations. Due

to the size of the matrices involved in the equation of motion, the pseudomodal method was used to reduce the dimension of the FEM model. For this aim, the reduction is achieved by changing from the physical coordinates x to modal coordinates q as follows:

$$x = \Phi q, \tag{2.2}$$

where Φ is the modal matrix containing the m first vibration modes of the nongyroscopic, symmetric and undamped associated rotor.

Substituting (2.2) into (2.1) and multiplying the resulting expression by Φ^T, the reduced equation of motion of the rotor is given by

$$\left[\widetilde{M}\right]\{\ddot{q}\} + \left[\widetilde{D} + \dot{\emptyset}\widetilde{G}\right]\{\dot{q}\} + \left[\widetilde{K} + \ddot{\emptyset}\widetilde{K}_{\text{st}}\right]\{q\} = \{Q\}, \tag{2.3}$$

where

$$\begin{aligned} &\left[\widetilde{M}\right] = \Phi^T[M]\Phi, \qquad \left[\widetilde{D}\right] = \Phi^T[D]\Phi\ , \qquad \left[\widetilde{G}\right] = \Phi^T[G]\Phi; \\ &\left[\widetilde{K}\right] = \Phi^T[K]\Phi, \qquad \left[\widetilde{K}_{\text{st}}\right] = \Phi^T[K_{\text{st}}]\Phi, \qquad [Q] = \Phi^T[F_{\text{ext}}]. \end{aligned} \tag{2.4}$$

The solution of (2.3) results in a response vector described in modal coordinates. By applying (2.2), it is possible to convert the dynamic response to physical coordinates.

3. Smart Spring Mechanism

Several applications of the SSM have been explored for vibration suppression in the last years. Daley et al. [10] developed a system based upon an electromagnet combined in parallel with passive elements for vibration suppression in marine structures, namely, the smart spring mounting system. The results demonstrated that only the rigid body modes of the machinery were controlled. Yong et al. [11] obtained successful results using a different SSM-patented concept based on two springs arranged in parallel. In their paper, it was demonstrated the concept ability for multiple harmonics vibration control of helicopter blades. Nitzsche et al. [12] presented the control efficiency of the same concept through numerical and experimental investigations. Furthermore, a feedback control system was used to improve the control efficiency. The architecture of the SSM used in the last two presented papers is conceptually shown in Figure 1.

If the friction between the PZT stack and the host structure is disregarded (normal force $N(t)$ = infinite and the friction $f(t) = 0$), the SSM behavior can be represented by two distinctly dynamic systems, according to the PZT stack status. The first one is active when the PZT is turned off, and the equivalent SSM stiffness is given by $k_{\text{ps}} + k_{\text{as}}$. The second status is obtained when the PZT is turned on. In this situation, the active spring is unattached leading the SSM to operate only through the primary spring k_{ps}. Note that if the friction is considered, the SSM becomes able to vary combinations of stiffness and damping at a particular location of the structure. Thus, the SSM mechanisms can actuate over a broadband of frequencies with low voltage requirement and displacement capability of the piezoelectric actuator [4]. It

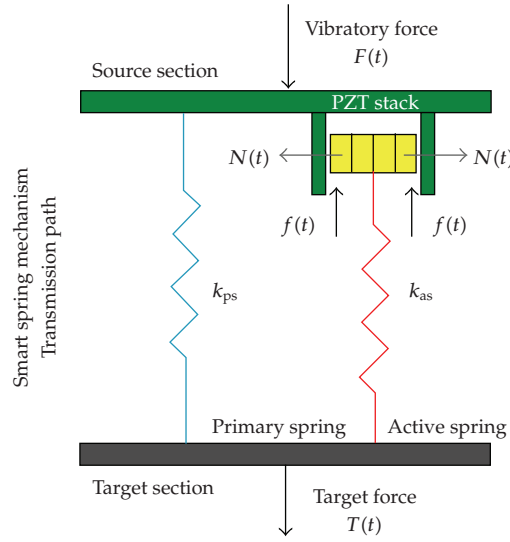

Figure 1: Smart spring concept (adapted from [4]).

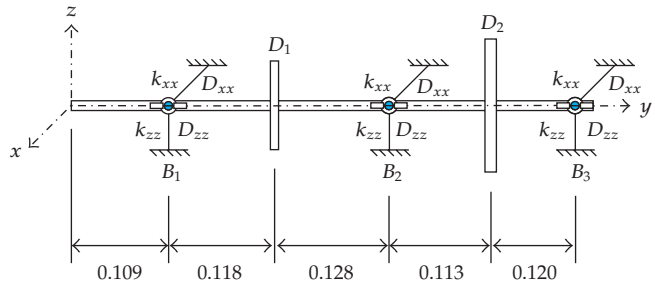

Figure 2: Rotor model.

is worth mentioning that most semi-active vibration control approaches are capable to change only a single structural property.

4. Applications

The proposed methodology was numerically applied to a rotor system composed of a horizontal flexible steel shaft, represented by 20 Timoshenko's beam elements, two rigid steel discs (D_1 and D_2), and three asymmetric bearings (Figure 2). The physic and geometric properties of the shaft, discs, and bearings are given in Table 1. The matrix equation of motion of the studied rotor was solved by using a MATLAB/SIMULINK code. The obtained responses were compared with the commercial software ROTORINSA for validation purposes. In all analyses performed in this study, only the displacement responses generated by the first ten vibration modes of the rotor measured along the x and z directions at the bearings positions were considered.

The proposed SSM on-off control strategy is based on instantly reductions in the stiffness of the bearings when the rotor gets close to a critical speed during its transient

Table 1: Physics and geometric properties of the rotor elements.

Rotor elements	Properties	Values
Shaft	Length (m)	0.588
	Diameter (m)	0.010
	Young's modulus (Pa)	2.0×10^{11}
	Density (Kg/m^3)	7800
Disc D_1	Thickness (m)	0.005
	Diameter (m)	0.100
	Young's modulus (Pa)	2.0×10^{11}
	Density (Kg/m^3)	7800
Disc D_2	Thickness (m)	0.010
	Diameter (m)	0.150
	Young's modulus (Pa)	2.0×10^{11}
	Density (Kg/m^3)	7800
Bearings B_1, B_2 and B_3	k_{xx} (N/m)	49.0×10^3
	k_{zz} (N/m)	60.0×10^3
	D_{xx} (Ns/m)	5.0
	D_{zz} (Ns/m)	7.0
Proportional damping $D = \alpha M + \beta K$	α	1.0×10^{-1}
	β	1.0×10^{-5}

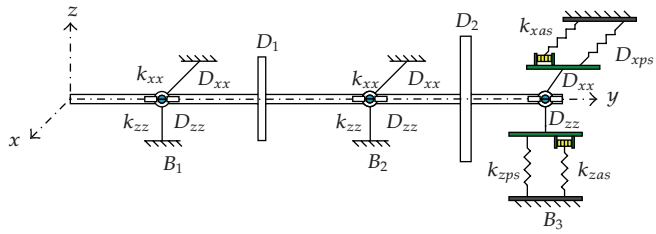

Figure 3: SSM locations at x and z directions of the bearing B_3.

rotation. This procedure is performed in order to change the position of the critical speed in the Campbell diagram and, consequently, to attenuate the vibration amplitudes generated at that particular rotation speed. For this aim, in this paper, two smart springs were installed along the x and z directions at the location of the bearing B_3(Figure 3)—the highest outputs amplitudes were measured at B_3—to control the vibration generated by the rotor in transient rotation from 0 to 3000 RPM, during 3.5 seconds. In this application, the target section of each SSM (see Figure 1) was attached to the ground, and only the stiffnesses k_{xx} and k_{zz} of the bearing B_3 were used as varying parameters, being the friction between the PZT stack and the host structure disregarded. Additionally, for design purposes the equivalent stiffness of each SSM, namely, $k_{xps} + k_{xas}$ related with the SSM installed along the x direction, and $k_{zps} + k_{zas}$ related with the SSM installed along the z direction, are equal to the stiffnesses k_{xx} and $k_{zz}$of the bearing B_3, respectively.

Figure 4 shows the regions where the PZT stack of the SSM installed along the z direction is either turned off, thus producing an equivalent stiffness associated with the z

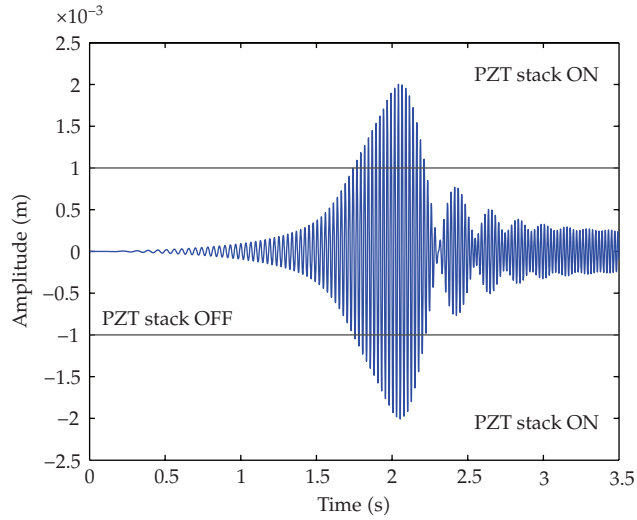

Figure 4: Equivalent SSM stiffness along the z direction related with the output amplitude.

direction of the bearing $B_3(k_{zps} + k_{zas})$, or turned on, so that the equivalent stiffness is simply k_{zps}. The same strategy is applied to the SSM along the x direction. Note that for the output amplitudes between 1.0×10^{-3} m and -1.0×10^{-3} m (outputs measured along the x and z directions of the bearing B_3) the PZT stack of each direction is in the off status. Outside of this range, the region delimited by the two lines, the PZT stack remains on. An important remark is that the choice of the SSM operation region is defined by the user, considering some key points such as, for instance, the desired vibration attenuation and the available electric power for the PZT stack.

The best choice of the SSM parameters k_{xps} and k_{xas} for the x direction and k_{zps} and k_{zas} for the z direction, which are associated with the control performance, was determined by using a multiobjective optimization procedure, as performed by the so-called compromise programming (CP). The unconstrained minimization of the scalar objective function was achieved by using a GA technique with an initial population of 200 individuals and 40 generations.

According to Vanderplaats [13], CP is able to combine various objective functions in order to obtain a reasonable compromise solution to many objectives. The compromise objective function is given by

$$F(x) = \left\{ \sum_{k=1}^{K} \left[\frac{W_k \{F_k(x) - F_k^*(x)\}}{F_k^w(x) - F_k^*(x)} \right]^2 \right\}^{1/2}, \tag{4.1}$$

where $F(x)$ is the CP objective function, W_k is the weighting factor assigned to the kth objective function, $F_k(x)$ is the kth objective function, $F_k^*(x)$ is the kth objective function target, and $F_k^w(x)$ is the worst known value of the kth objective function. In this paper, the $F_k^*(x)$ was determined by the optimization of each objective function considered independently, and $F_k^w(x)$ was associated to the worst configuration. CP was performed combining the norm and the maximum absolute value of the responses measured at the bearings positions, measured

Table 2: Results obtained by the minimization processes.

Direction	Objective	P	k_{as} (N/m)	k_{ps} (N/m)
x	Norm	0.6395	31335.5	17664.5
	Maximum	0.6260	30674.0	18326.0
	N_b	0.9589	46986.1	2013.9
	CP	0.6507	31884.3	17115.7
z	Norm	0.8095	48570.0	11430.0
	Maximum	0.4831	28986.0	31014.0
	N_b	0.9101	54606.0	5394.0
	CP	0.7052	42312.0	17688.0

Table 3: SSM control efficiency (response RMS values).

Directions/bearings	Without SSMs (10^{-3})	With SSMs (10^{-3})	Difference (%)
x/B_1	0.1285	0.0984	−23.42
x/B_2	0.3818	0.2255	−40.93
x/B_3	0.4109	0.2581	−37.17
z/B_1	0.1369	0.1008	−26.38
z/B_2	0.4576	0.2919	−36.21
z/B_3	0.4749	0.3210	−32.41

along the x and z directions, and the total number of activation times, N_b, which each PZT stack is turned on. The weighting factors W_k related with the two first indexes were chosen as equal to 1.0 and the third one was chosen as equal to 1.5. These indexes were minimized considering the design variable P_x and P_z ($0 < P_x < 1$ and $0 < P_z < 1$), being $k_{xas} = P_x k_{xx}$ and $k_{zas} = P_z k_{zz}$. Table 2 presents the SSM parameters found in the minimization process.

Note that the results for CP show that the stiffness reduction provided by the SSM installed along the x direction was as big as 65.07% and 70.52% along the z direction, abrupt reductions that could generate instability in the rotor motion. However, Figure 5 shows through the outputs measured along the x and z directions at the position of the bearings that the rotor keeps stable despite the large stiffness reductions imposed to the rotor. This behavior can be explained by the amount of damping in the system. Additionally, Figure 5 compares the dynamic responses for the rotor without and with the SSMs. The control performance appears to be efficient along the both directions at all the positions where a bearing is placed to support the rotor. This means that the SSMs are efficient not only at the point to which the SSMs were attached (bearing B_3).

In order to demonstrate quantitatively the SSM control efficiency, Table 3 shows the RMS value (Root Mean Square) of the outputs obtained for the rotor without and with the SSMs. One can note that the vibration attenuation is efficient along both directions of the bearing B_3 (greater than 30%), as shown in Figure 5. Expressive vibration attenuation is observed also at the bearings B_1 and B_2.

Another aspect of the SSM technology presented in this paper is related to the design of ecologically correct machines. Removing N_b from the optimization process, the PZT stack of the z direction is turned on 50 times. When the energy consumption is considered in the process (case presented in Figure 5 and Table 3), this number decreases to 36 (28% of reduction). For the x direction, this number remained approximately constant (reduction from 34 to 33 times).

Table 4: SSM control efficiency of the ecorotor.

Directions/bearings	Ecorotor (10^{-3})	Norm and maximum (10^{-3})	Difference (%)
x/B_1	0.0984	0.0966	1.8394
x/B_2	0.2255	0.2266	−0.4750
x/B_3	0.2581	0.2595	−0.5051
z/B_1	0.1008	0.0952	5.9292
z/B_2	0.2919	0.2732	6.8444
z/B_3	0.3210	0.3071	4.5213

Additionally, supporting the adoption of the ecorotor concept in the design of machines and systems, Table 4 shows the RMS values of the rotor response. This means that including the energy consumption in the optimization process does not alter significantly the efficiency of the control. However, the amount of energy consumed by the system is reduced for this configuration.

Previous results showed the efficiency of the SSM with respect to vibration reduction of a rotor that crosses critical speeds during its transient rotation. However, rotating machines are also susceptible to external disturbances, such as impact. Therefore, it is necessary to evaluate the SSM influence for this kind of excitation. Figure 6 shows the behavior of the rotor subjected to impacts applied along the x and z directions at the position of the disc D_2 when $t = 1.75$ sec. The dynamic responses of the rotor with the SSMs are then presented in Figure 6. The rotor is accelerating from 0 to 3000 RPM, similarly to the previous case. It is possible to observe significant differences between the outputs obtained with and without impact (refer to Figure 5).

However, one can see that the rotor motion is kept stable when the SSMs are operating, which means that the behavior of the system with the SSMs is robust to external disturbances during the transient motion of the rotor. The same evaluation was performed for the rotor under steady state condition at 3000 RPM as depicted in Figure 7. Here again, impacts were applied along the x and z directions at the position of the disc D_2 when $t = 1.75$ sec. It is possible to observe significant differences between the outputs obtained with and without the impacts disturbances. However, as in the previous cases, the rotor motion remains stable when the SSMs are operating due to the amount of damping in the system. This indicates that the system with SSMs operating under steady-state condition is robust to external disturbances.

Finally, the influence of the SSMs was evaluated for the rotor at rest. Figure 8 shows the output measured when the rotor was excited by impacts applied along the x and z directions at the position of the disc D_2 when $t = 1.75$ sec. Note that when the SSMs are operating, the maximum output amplitude is 2.0×10^{-3} m (Figure 8(e)).

However, one can conclude that the difference founded between the cases with the rotor in rotation and the one with the rotor at rest is associated with the damping.

It is worth mentioning that other ranges can be used to activate the smart spring (see Figure 4). For example, if the value of the amplitude response is reduced to 0.5×10^{-3} m the optimal stiffness values result very much, that is, the system becomes very flexible (the first critical speed is reduced significantly). Also, the strategy to cross the critical speed safely could be reached by increasing the stiffness of the system so that the first critical speed would move to a higher rotation. As this is an exploratory study, the results shown aim at demonstrating the potential use of smart springs in rotor dynamics.

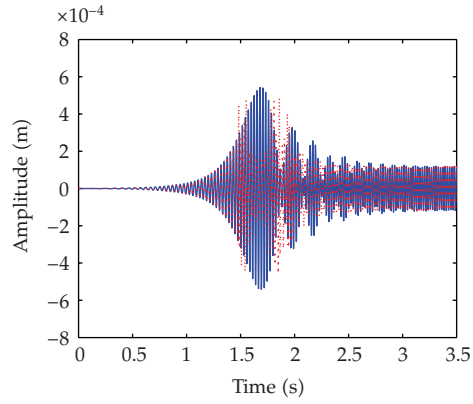

(a) Output measured along the x direction of the bearing B_1

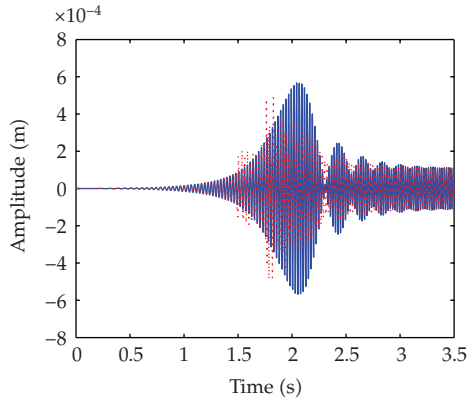

(b) Output measured along the z direction of the bearing B_1

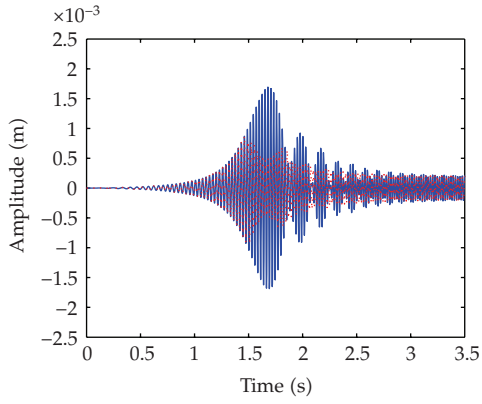

(c) Output measured along the x direction of the bearing B_2

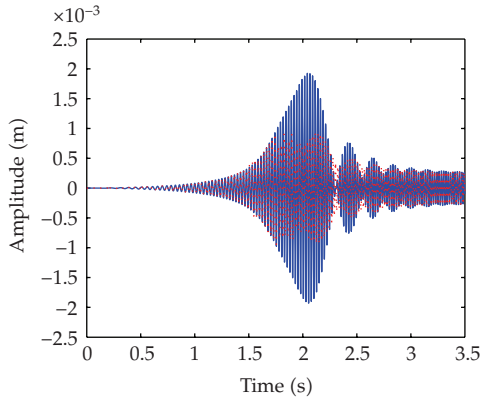

(d) Output measured along the z direction of the bearing B_2

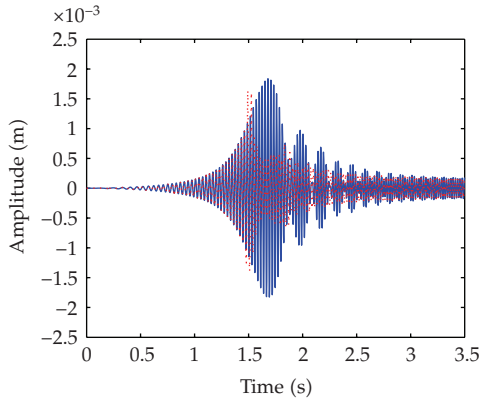

(e) Output measured along the x direction of the bearing B_3

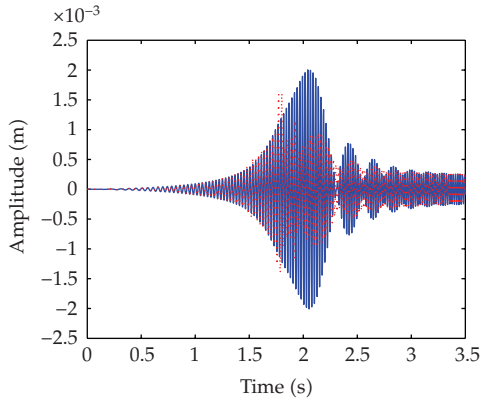

(f) Output measured along the z direction of the bearing B_3

Figure 5: Dynamic responses calculated for the rotor without and with the SSM.

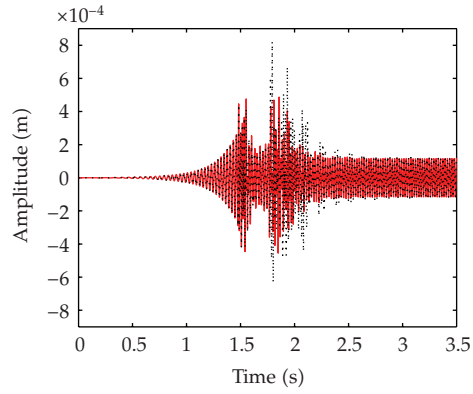

(a) Output measured along the x direction of the bearing B_1

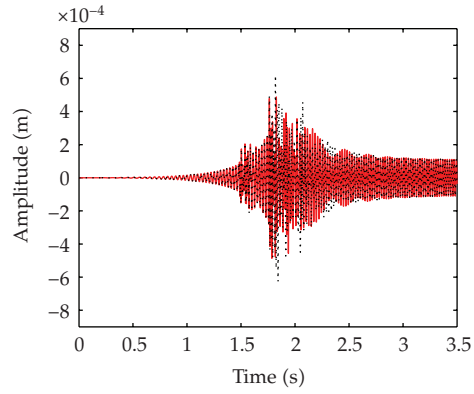

(b) Output measured along the z direction of the bearing B_1

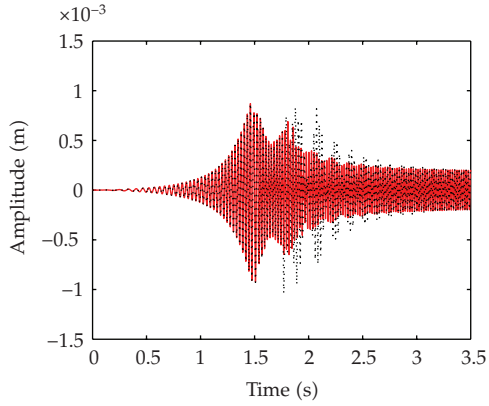

(c) Output measured along the x direction of the bearing B_2

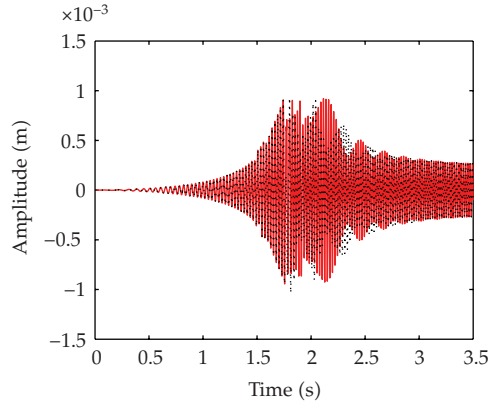

(d) Output measured along the z direction of the bearing B_2

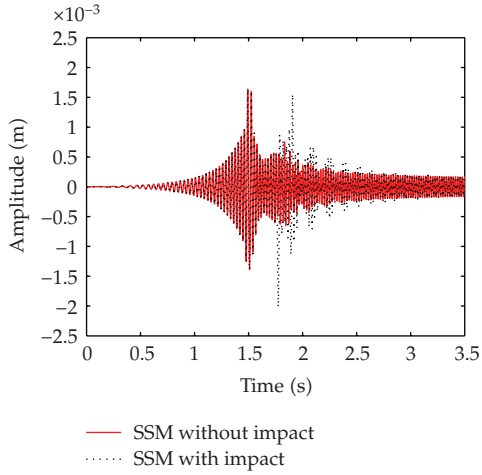

(e) Output measured along the x direction of the bearing B_3

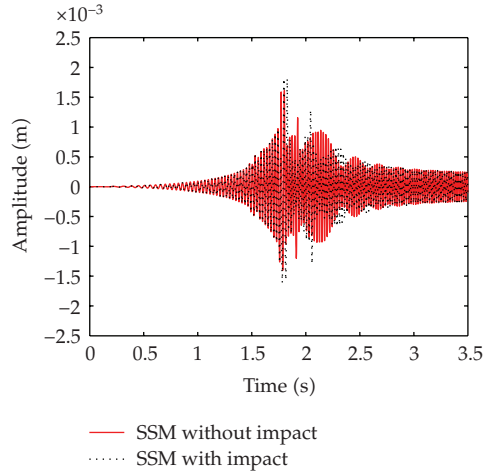

(f) Output measured along the z direction of the bearing B_3

Figure 6: Output responses measured for the rotor with and without impact during the transient rotation.

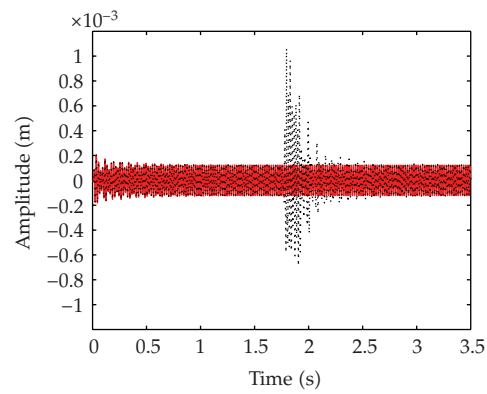

(a) Output measured along the x direction of the bearing B_1.

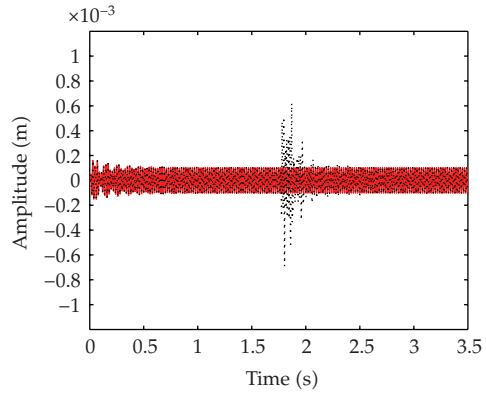

(b) Output measured along the z direction of the bearing B_1.

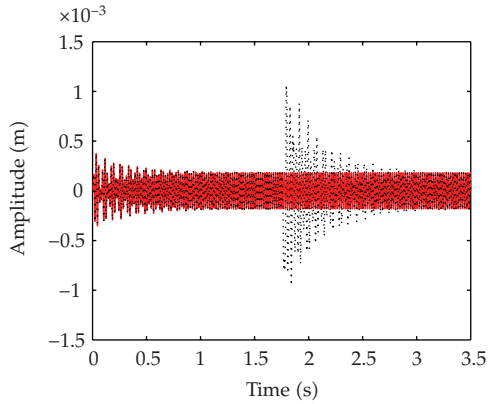

(c) Output measured along the x direction of the bearing B_2.

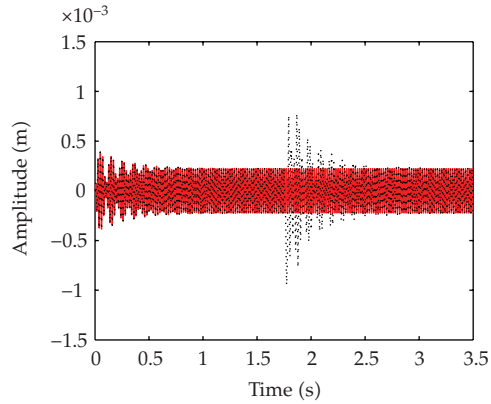

(d) Output measured along the z direction of the bearing B_2.

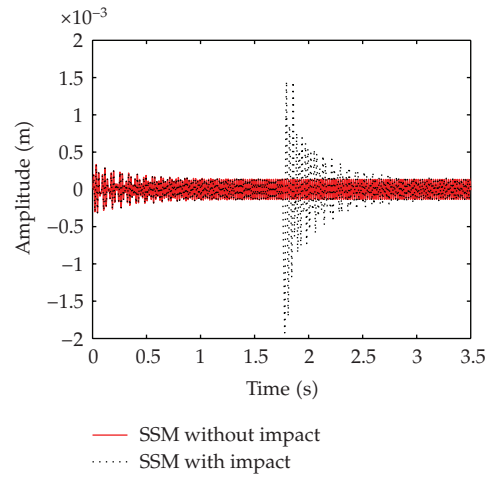

(e) Output measured along the x direction of the bearing B_3.

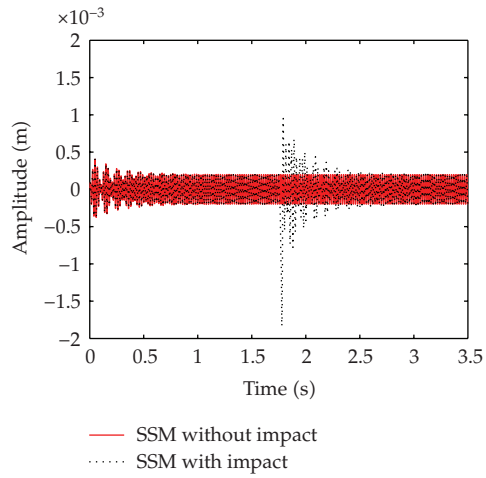

(f) Output measured along the z direction of the bearing B_3.

Figure 7: Output responses measured for the rotor with and without impact for steady state rotation.

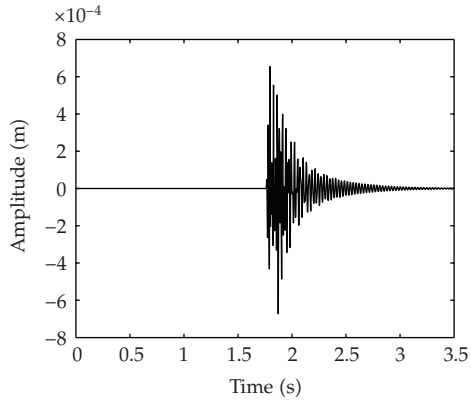

(a) Output measured along the x direction of the bearing B_1.

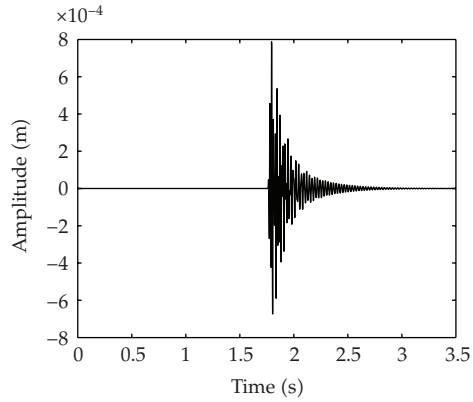

(b) Output measured along the z direction of the bearing B_1.

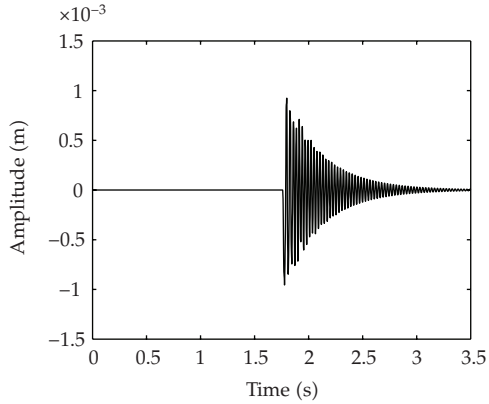

(c) Output measured along the x direction of the bearing B_2.

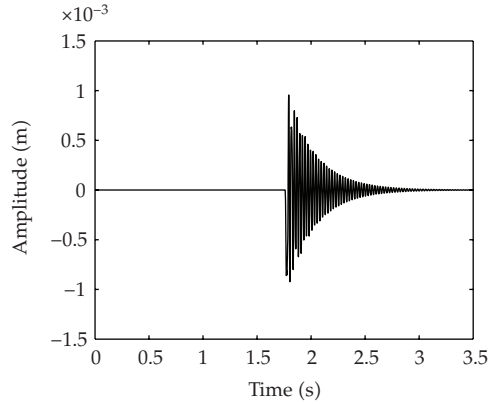

(d) Output measured along the z direction of the bearing B_2.

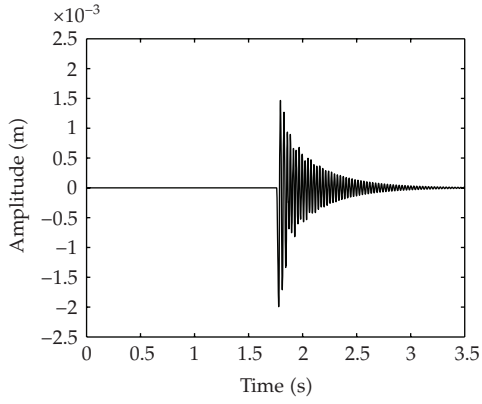

(e) Output measured along the x direction of the bearing B_3.

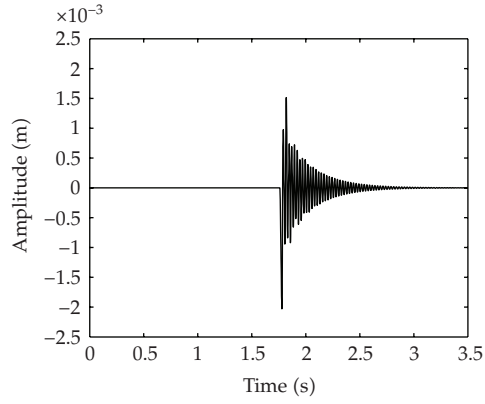

(f) Output measured along the z direction of the bearing B_3.

Figure 8: Output responses measured for the rotor at rest excited by an impact force.

5. Conclusions

In this paper, a vibration attenuation technique based on SSM for rotating machines that cross critical speeds during its transient rotation was evaluated. The proposed approach presented promising results, leading to reductions as large as 30% for the case in which the parameters of the SSM were optimized. The optimization process was conducted using a GA technique that was applied to a multi-objective problem. Despite the stiffness reduction (around 65%) imposed to the rotor by the SSM, mathematical simulation results indicate that the system did not become unstable during the test. The robustness of the approach with respect to external disturbances was analysed. First, an impact force was applied to the rotor disc during the transient rotation. In the second case, the rotor was evaluated for steady state conditions (constant rotation) and, finally, the system vibration was analysed for the rotor at rest. For the three cases considered, the results showed that the on-off control technique is robust to external disturbances. Additionally, it was possible to conclude that the inclusion of the concept of ecorotors in the design of the controller did not reduce significantly the SSM efficiency while reducing the amount of energy in the controller. The proposed approach seems to be very effective to reduce vibrations for different operating conditions of the rotor. Further work includes the modelling of the friction of the PZT stack inside the SSM so that the stiffness and damping of the system can be altered simultaneously. Also, the technique will be implemented experimentally.

Acknowledgment

The authors are thankful to the Brazilian Research Agencies FAPEMIG, CNPq, and CAPES for the financial support to this work through the INCT-EIE.

References

[1] J. Mahfoud, J. Der Hagopian, N. Lévecque, and V. Steffen Jr., "Experimental model to control and monitor rotating machines," *Mechanism and Machine Theory*, vol. 44, no. 4, pp. 761–771, 2009.

[2] R. C. Simões, V. Steffen Jr., J. Der Hagopian, and J. Mahfoud, "Modal active vibration control of a rotor using piezoelectric stack actuators," *Journal of Vibration and Control*, vol. 13, no. 1, pp. 45–64, 2007.

[3] D. J. Inman, *Engineering Vibration*, Prentice-Hall, Upper Saddle River, NJ, USA, 2001.

[4] V. Wickramasinghe, Y. Chen, and D. Zimcik, "Experimental evaluation of the smart spring impedance control approach for adaptive vibration suppression," *Journal of Intelligent Material Systems and Structures*, vol. 19, no. 2, pp. 171–179, 2008.

[5] Y. Skladanek, J. Der Hagopian, and J. Mahfoud, "Energy cost assessment of the active control of a rotating machine by using an electromagnetic actuator and a piezoelectric actuator," in *Proceedings of the ASME Gas Turbine Technical Congress & Exposition*, vol. 6, pp. 847–854, Orlando, Fla, USA, June 2009.

[6] D. Guyomar, C. Richard, and S. Mohammadi, "Semi-passive random vibration control based on statistics," *Journal of Sound and Vibration*, vol. 307, no. 3–5, pp. 818–833, 2007.

[7] F. Matichard and L. Gaudiller, "Improvement of potential energetic exhange using non linear control," in *Proceedings of the IEEE/ASME International Conference on Advanced Intelligent Mechatronics (AIM '05)*, pp. 807–812, 2005.

[8] E. H. Maslen, P. E. Allaire, M. D. Noh, and C. K. Sortore, "Magnetic bearing design for reduced power consumption," *Journal of Tribology*, vol. 118, no. 4, pp. 839–846, 1996.

[9] M. Lalanne and G. Ferraris, *Rotordynamics Prediction in Engineering*, John Wiley & Sons, New York, NY, USA, 2nd edition, 1998.

[10] S. Daley, F. A. Johnson, J. B. Pearson, and R. Dixon, "Active vibration control for marine applications," *Control Engineering Practice*, vol. 12, no. 4, pp. 465–474, 2004.

[11] C. Yong, D. G. Zimcik, V. K. Wickramasinghe, and F. Nitzsche, "Development of the smart spring for active vibration control of helicopter blades," *Journal of Intelligent Material Systems and Structures*, vol. 15, no. 1, pp. 37–47, 2004.

[12] F. Nitzsche, T. Harold, V. K. Wickramasinghe, C. Yong, and D. G. Zimcik, "Development of a maximum energy extraction control for the smart spring," *Journal of Intelligent Material Systems and Structures*, vol. 16, no. 11-12, pp. 1057–1066, 2005.

[13] G. N. Vanderplaats, *Numerical Optimization Techniques for Engineering Design*, Vanderplaats Research & Development, Inc., Colorado Springs, Colo, USA, 4th edition, 1999.